Parameterization of the Effect of Cloud Condensation Nuclei on Optical Properties of a Non-precipitating Water Layer Cloud

Naomi KUBA, Hironobu IWABUCHI

Frontier Research System for Global Change, Yokohama, Japan

Ken-ichi MARUYAMA

National Research Institute for Earth Science and Disaster Prevention, Tsukuba, Japan

Tadahiro HAYASAKA

Research Institute for Humanity and Nature, Kyoto, Japan

Takao TAKEDA

Tottori University of Environmental Studies, Tottori, Japan

and

Yasushi FUJIYOSHI

Frontier Research System for Global Change, Yokohama, Japan
Institute of Low Temperature Science, Hokkaido University, Sapporo, Japan

(Manuscript received 2 September 2002, in revised form 10 January 2003)

Abstract

A new method is proposed to predict the optical thickness, effective radius, and concentration of cloud droplets in water layer clouds by using the spectrum of cloud condensation nuclei (CCN), ascent velocity at cloud base, and liquid water path (LWP). A retrieval method is also proposed to predict CCN number concentration by using independent observational data of ascent velocity at the cloud base, the optical thickness and LWP of clouds.

For this purpose, a newly developed cloud microphysical model that relates cloud droplet size distributions to the updraft velocity, and to CCN constituents and size distribution is used. Cloud droplet growth is calculated, with special care being taken to avoid non-physical numerical diffusion of the droplet spectrum.

Near the cloud base, CCN activation and subsequent cloud droplet growth are calculated in a Lagrangian framework to model the effect of CCN on growth by condensation more accurately. In the middle and upper parts of the cloud, an Eulerian framework is used to estimate growth by coalescence for cloud droplet size distributions. Simulated vertical profiles of droplet size distributions, and a solu-

Corresponding author: Naomi Kuba, Frontier Research System for Global Change, 3173-25 Showa-machi, Kanazawa-ku, Yokohama 236-0001, Japan.
E-mail: kuba@jamstec.go.jp

tion to the radiative transfer equation using the discrete ordinate method, with no parameterizations, yield the optical properties of the cloud for short-wavelength radiation.

Using the approximation equation proposed in this study, the maximum value of supersaturation in a cloud (S_{max}) is predicted by observing cumulative activated CCN number concentration at 0.075% supersaturation ($N_c(0.075\%)$), and the ascent velocity at the cloud base. Using this S_{max}, we can estimate $N_c(S_{max})$, which is the cumulative number concentration of CCN, whose critical supersaturations are lower than S_{max}. $N_c(S_{max})$ is used to predict the concentration of cloud droplets at the middle altitude of layer cloud (N_d). Conventionally N_d is assumed to be $N_c(S_{max})$. However, our parameterization can show that N_d is smaller than $N_c(S_{max})$, when $N_c(S_{max})$ is large. For the fixed liquid water path, optical thickness and effective radius can be expressed as a function of N_d, unless drizzle is falling from the cloud. The parameterizations developed in this paper are based on the U.S. Standard Atmosphere 1976. If necessary, the parameterizations for the extremely different atmosphere from that used here can be developed in the same way.

1. Introduction

Identifying the effect of aerosols on the atmospheric radiative budget is one of the keys to understanding and predicting global climate change. Twomey (1974, 1977) noted the importance of the indirect effect of aerosols, which is that increased pollution leads to an increase in clouds' optical thickness and albedo. Twomey (1991) also showed that relatively modest anthropogenic influences could modify the reflectance of stratus decks, and that satellite data commonly show reflectance increasing by about 0.2 across ship tracks, which is attributed to cloud condensation nuclei (CCN) emissions from the ships.

IPCC (2001) indicated that estimation of the indirect radiative forcing, that is due to all tropospheric aerosols, is still subject to a very low level of scientific understanding (LOSU), and that one of the major uncertainties in this respect arises from the quantification of aerosol-cloud interaction. Given the size distribution of cloud droplets, their effective radius, and the liquid water path (LWP), the optical properties of a cloud can be estimated by using the parameterization scheme presented by Stephens (1978). However, it is apparent that the size distribution of cloud droplets is affected by CCN properties. Thus, a quantitative estimate of the effect of CCN on the optical properties of clouds is needed.

Stratus and stratocumulus clouds in the boundary-layer are important as a modulator of the earth's energy budget, because of their high albedos and the large areas they cover. Slingo (1989) showed that the sensitivity of the reflectance of clouds to both the effective droplet radius and the LWP, decreases as the LWP increases, and implied that the influence of microphysical structure and cloud thickness on the shortwave radiative properties of clouds will be greatest for clouds with a LWP between about 10 and 100 g m^{-2}. According to the observations summarized by Fourquart et al. (1990), the LWP of stratus and stratocumulus clouds ranges between roughly 10 and 200 g m^{-2}. Therefore, our study addresses layer clouds with a LWP thinner than 100 g m^{-2}. Since drizzle does not usually accompany these clouds, the adiabatic parcel model is available to study the effect of CCN on their optical properties.

Martin et al. (1994) proposed the parameterization for the effective radius of droplets in layer clouds as a function of the number concentration of droplets. The number concentration of droplets is parameterized as a function of the aerosol concentration in the radius size range of 0.05–1.50 μm. Brenguiter et al. (2000) verified their parameterization of the optical thickness of clouds as a function of cloud droplet number concentration and the LWP, by using in situ measurements of microphysical parameters in stratocumulus. In our study, the parameterizations for the optical thickness of layer clouds and cloud droplet effective radius are developed as a function of cloud droplet number concentration and LWP, and the parameterizations for cloud droplet number concentration are also developed as a function of the cumulative number of CCN and ascent velocity near the cloud base.

The purpose of this study is to propose approximate equations for predicting changes in the optical properties of a cloud caused by

changes in the properties of CCN. For this purpose, we developed a cloud microphysical adiabatic parcel model that incorporates the effects of both the ascent velocity of air parcels and the CCN spectrum on the size distribution of cloud droplets. Some CCN in the ascending air parcel are activated and then grow to form cloud droplets; others remain as wet CCN. The number of activated CCN, and resultant cloud droplets, determines the microphysical and optical properties of the cloud. Our numerical model calculates the growth of nuclei by condensation in a Lagrangian framework until the nuclei can be clearly identified as activated nuclei and embryos. This process is important for an accurate estimation of the concentration of activated nuclei. We also give special attention to calculating cloud droplet growth, in order to avoid numerical diffusion and to include the solute effect on cloud droplets. The short-wavelength radiative properties (optical thickness and reflectance) of simulated clouds are computed using simulated vertical profiles of droplet size distribution.

Feingold et al. (1997) carefully examined the impact of drop spectral broadening on optical properties by using Twomey's (1959) relationship to estimate the number of activated CCN, $N_{act} = CS^k_{max}$. This relationship tends to overestimate the number of activated CCN, or the number of cloud droplets. In this study, it is shown that even after growing beyond their critical radii, some CCN revert to being inactivated after supersaturation has reached its maximum value. Chuang et al. (1997) and Yun and Hudson (2002) also noted this overestimation, which is caused by assuming that the cloud droplet concentration is equal to the concentration of CCN for which critical supersaturation is lower than the maximum supersaturation in the cloud. In our model, the emphasis is on precise estimation of the final number of activated CCN.

We studied how the effect of anthropogenic aerosols on the optical properties of clouds varies as a result of differences in background CCN, because Taylor et al. (2000), using data from the Monterey Area Ship Track (MAST) experiment, found that the impact of aerosols emitted from ships was strongly dependent on the microphysical conditions of the background cloud.

Integrating the results of the simulation using the model, we developed the parameterization to predict cloud droplet number concentration (N_d) as a function of cumulative number concentration of CCN and ascent velocity at the cloud base, and the parameterization to predict the optical thickness of a cloud as a function of N_d and LWP. A retrieval method was also proposed to predict CCN number concentration by using independent observational data of ascent velocity at cloud base, the optical thickness and LWP of clouds. Obtaining information of CCN number concentration globally in this way is extremely useful. Although conventional remote sensing data provides information on aerosol particles (Higurashi et al. 2000; Nakaijma et al. 2001), information on CCN is needed in order to examine the indirect radiative forcing of aerosol particles. Therefore, a retrieval method for predicting the cumulative number concentration of CCN using observational data has also been developed in this study.

2. Cloud model

Chen and Lamb (1994) developed a detailed microphysical and chemical cloud model and simulated the formation of orographic clouds (Chen and Lamb 1999) to show that the size distribution of aerosols has a significant influence on both warm- and cold-cloud processes. Our model is simpler than theirs, but it can estimate the concentration of activated CCN and the size distribution of cloud droplets; it also allows close examination of the relationship between CCN and the optical properties of layer clouds through the use of the Lagrangian framework. Our model is similar to that developed by Cooper et al. (1997), which used variable bins and the modified Kovetz-Olund algorithm (Kovetz and Olund 1961) to calculate the growth of droplets by condensation and coalescence. In contrast, our model uses fixed bins and the advection algorithm developed by Bott (1989) to determine condensational growth, and uses the flux method developed by Bott (1998) to estimate growth by coalescence. Fixed bins are adequate for estimating the settling of droplets, as will be noted in a follow-up paper that is presently in preparation.

The method of subdividing the discretization of the CCN size distribution also affects the re-

sults of calculation. Takeda and Kuba (1982) noted that the discretizations of Mordy (1959) and Fitzgerald (1974) were too broad to allow an accurate estimation of cloud droplet concentration. In our model, the number of nuclei included in one class is less than 1% of the number of activated cloud droplets. Consequently, the error in the concentration of activated cloud droplets is limited to 1%.

Our cloud model describes the formation of cloud droplets around CCN, and the subsequent growth of the droplets by condensation and coalescence. We calculate the condensational growth of nuclei in a Lagrangian framework that includes surface kinematics. Thus, the model does not cause the overestimation of the cloud droplet concentration that is caused by assuming that the cloud droplet concentration is equal to the concentration of CCN activated at the maximum supersaturation in the cloud.

2.1 Assumptions

Consider an air parcel that contains CCN and water vapor, ascending in the U.S. Standard Atmosphere 1976, without exchanging heat or moisture with its environment. We do not calculate the ascent velocity, but give a vertical profile of the updraft velocity.

Considering the time constants at which CCN reach their equilibrium radii in the ambient humidity (100% at cloud base), CCN smaller than 0.1 μm in radius, and CCN larger than 1 μm in radius, are initially assumed to be in equilibrium at 99% and 90% RH, respectively. Intermediate CCN are initially assumed to be in equilibrium between 99 and 90% RH as a function of radius.

The model ignores the effect of soluble gases, following the idea, as in Laaksonen et al. (1998), that the traditional form of the Köhler equation may be correct for clouds formed from small particles of highly soluble substances (e.g., NaCl, $(NH_4)_2SO_4$, H_2SO_4), and giant sea-salt nuclei. Entrainment, or surface tension changes, due to organics, are ignored for simplicity. In numerous previous studies, entrainment has been a mechanism for broadening the droplet size spectrum. However, Hudson and Yum (1997) found scant evidence for broadening due to entrainment, except for the activation of small droplets. They suggested that broad spectra might be due simply to variations in CCN spectra and updraft velocities. The activation of CCN introduced by entrainment can affect the optical properties of clouds. However, for layer clouds in which updraft velocities do not exceed a few meters per second, new activation rarely occurs unless the original CCN concentration near the cloud base is extremely small. Hence, adiabatic modeling is a reasonable approach to employ for discerning the effect of CCN on the optical properties of layer clouds.

All CCN and cloud droplets are assumed to move with and remain in the air parcel. This assumption leads the concentration of large droplets overestimated. The error, which is caused by neglecting dropping out of droplets from air parcel, is larger in thicker cloud, so we limit the model to clouds thinner than 300 m and 100 g m^{-2} in LWP. In spite of the neglect of the dropping out of droplets from the air parcel, coalescence growth of droplets caused by the difference in falling velocity among droplets is taken into account.

2.2 Governing equations

The equations governing the growth rate of droplets by condensation are those in Takeda and Kuba (1982). The potential temperature tendency of an air parcel is calculated. The equation governing the coalescence-forced rate of change of the cloud droplet spectrum over time is stochastic. Collision efficiency is computed from Table 1 in Hall (1980).

2.3 Computational scheme

Two computational schemes are adopted in this model (see Table 1). In the layer near the cloud base, a Lagrangian formulation is used to estimate CCN activation, so as to avoid the numerical diffusion of cloud droplet size distribution that occurs when condensational growth is calculated in an Eulerian framework. An Eulerian approach is used to estimate the coalescence growth of cloud droplets in the middle and upper parts of the cloud, because calculation of coalescence growth in a Lagrangian framework is difficult and time consuming (e.g., the Monte Carlo method). Special care is taken to limit numerical diffusion in the Eulerian approach, and to make a smooth transition between the two schemes. This combination of schemes yields correct results provided that

Table 1. The two computational schemes.

Layer	Near the cloud base	Middle and upper
Framework	Lagrangian	Eulerian
Fixed values	n_j Concentration of CCN included in each class. ($j = 1, \ldots, 165$)	$r_i = r_1 2^{(i-1)/3k}$ Representative radius of droplets included in each bin. ($i = 1, \ldots, 200$)
Variable values	$r_j(t)$ Radius of droplets forming on CCN included in each class.	$n_i(t)$ Concentration of droplets included in each bin.
Activation	Takeda and Kuba (1982)	not considered
Condensation	Takeda and Kuba (1982)	DL-method
Coalescence	not considered	Bott's (1998) method
Δt	0.01–0.1 s	2.0 s

CCN activation does not occur in the middle and upper parts of a cloud, which may happen if new CCN are introduced into a cloud by entrainment.

a. The Lagrangian framework in the layer near the cloud base

CCN activation and the initial growth of cloud droplets by condensation are computed in a Lagrangian framework that incorporates the solute effect of CCN. An advantage of this method is that numerical diffusion of droplet size distribution is avoided. The Lagrangian framework is implemented from the cloud base up to 50 m above the base. CCN size distribution is approximated using discrete radii classes; initial values are chosen prudently. The number of nuclei included in one class is less than 1% of the number of activated cloud droplets, so as to limit the error in the concentration of activated cloud droplets to 1%. For this study, CCN (up to 10 μm in radius) are partitioned into 165 separate classes, of which more than 100 classes can become activated and evolve into cloud droplets. The initial minimum radius of a CCN must be smaller than the radius of the smallest CCN that can be activated, since the simulated results would be invalid if all of the CCN were activated. The time evolution of the representative droplet radius in each class is calculated as detailed in Takeda and Kuba (1982).

As mentioned by Fitzgerald (1974) and Robinson (1984), a very small time step is needed to estimate the growth of small nuclei by condensation accurately. The time step in this model is based on the radius of the smallest activated nuclei. When there are low concentrations of CCN and a high ascent velocity, a very small time step is required; if smaller nuclei cannot be activated, the time step can be larger. The time step used in this model varies between 0.01 and 0.1 seconds. In addition, the growth by condensation of each droplet during each step is limited so that the radius of each droplet cannot exceed its equilibrium radius.

b. The Eulerian framework in the middle and upper cloud layers

The cloud droplet size distribution in the middle and upper parts of a cloud (defined as those layers more than 50 m above the cloud base) is expressed in an Eulerian framework, using representative radii bins $r_i = r_1 2^{(i-1)/3k}$, where k represents the fineness of classification. The concentration of droplets whose radii are between $(r_i - \Delta r_{i-})$ and $(r_i + \Delta r_{i+})$ is expressed as n_i, and the time evolution of n_i is computed.

Droplets in the bins grow by coalescence, modeled using a flux method developed by Bott (1998) that conserves mass and has little numerical diffusion. Cloud droplet growth by condensation is calculated using an advection algorithm based on Bott's (1989) method, except that the polynomial approximation is replaced with two straight lines joined at the center of the bin. Special attention is given to preventing numerical diffusion of the cloud droplet spectrum, and this method (the dual-linear line

method, hereafter the DL-method) has little numerical diffusion (see APPENDIX). The DL-method is simpler than the mixing ratio advection scheme developed by Walcek and Aleksic (1998), but nevertheless accurately estimates the condensation-forced time evolution of the cloud droplet size distribution.

The solute effect on cloud droplet growth by condensation is not considered here, but this simplification introduces little error because almost all cloud droplets are dilute, with the exception of droplets formed on rare, large CCN. The condensational growth rate $(dr/dt)_{cond}$ is much smaller than r for these rare droplets, which grow mostly by coalescence, so underestimation of their growth rate from condensation alone does not significantly affect estimates of their overall growth rate.

In this paper, the DL-method is used, adopting $k = 6$, yielding 200 droplet bins with radii ranging from 1.0 to 2128.4 μm. The model time step was 2.0 seconds.

2.4 *Numerical experiments*

The numerical experiments included 171 cases, combining nine vertical profiles of ascent velocity and 19 CCN spectra. The nine vertical profiles of ascent velocity are shown in Fig. 1. Cloud base is at an altitude of 500 m. Three vertical profiles of ascent velocity (maximum velocities of 0.4, 0.2, and 0.1 m s^{-1}, and respective velocities at the cloud base of 0.24, 0.12, and 0.06 m s^{-1}) were prepared for three cloud depths: 300 m (**a**, **b**, and **c**), 250 m (**d**, **e**, and **f**) and 200 m (**g**, **h** and **i**). The vertical velocities at the cloud base are chosen by referring to the observations by Hudson and Li (1995). The cloud depths are equivalent to LWPs of 100, 70 and 44 g m^{-2}, respectively. Figure 2a shows the 19 CCN supersaturation spectra. To cover the variety of natural CCN spectrum, four shapes of CCN spectrum are chosen, as shown in Fig. 2a (A, B, C and D). The numbers following A, B, C, and D in the figure represent the ratios of the concentration to A1.0, B1.0, C1.0, and D1.0, respectively. For example, A5.0 has the same shape as A1.0, but the number concentration of A5.0 is five times that of A1.0.

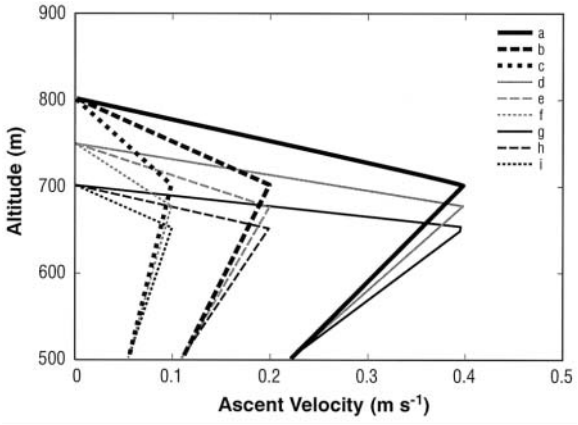

Fig. 1. Vertical profiles of ascent velocity. The cloud base is at 500 m. Cloud depth is 300 m (**a**, **b**, and **c**), 250 m (**d**, **e**, and **f**), or 200 m (**g**, **h**, and **i**). Maximum velocities are 0.4, 0.2, and 0.1 m s^{-1}, the velocities at the cloud base are 0.24, 0.12, and 0.06 m s^{-1}.

In 51 cases, we also examined the effect of artificial CCN on optical properties by including different amounts of small particles ($r < 0.1$ μm) or giant particles ($r > 1$ μm) with maritime CCN and continental CCN. Figure 2b shows the size distribution of continental CCN, made by transforming A5.0 in Fig. 2a assuming a chemical makeup of $(NH_4)_2SO_4$. The size distribution of maritime CCN is also shown. The concentration of small particles ($r < 0.1$ μm) of maritime CCN is smaller than that of continental CCN, and the concentration of giant particles ($r > 1$ μm) of maritime CCN is larger than that of continental CCN.

In all cases, the CCN were assumed to be NaCl or $(NH_4)_2SO_4$, typical soluble constituents in CCN. As the CCN supersaturation spectrum is the important factor determining the microstructure of clouds, differences in the soluble constituents of nuclei do not lead to large differences in the microstructure of clouds.

3. Radiative transfer model

The reflectance of layer cloud was calculated using the radiative transfer code, as developed by Nakajima and Tanaka (1986, 1988), which uses the discrete ordinates method. A U.S. standard atmosphere 1976 is assumed, and profiles of the concentration of the absorbing gas are included. Gaseous absorption was incorporated with a three-term k-distribution, using absorption coefficients compiled in the LOWTRAN-7 database (Kneizys et al. 1988).

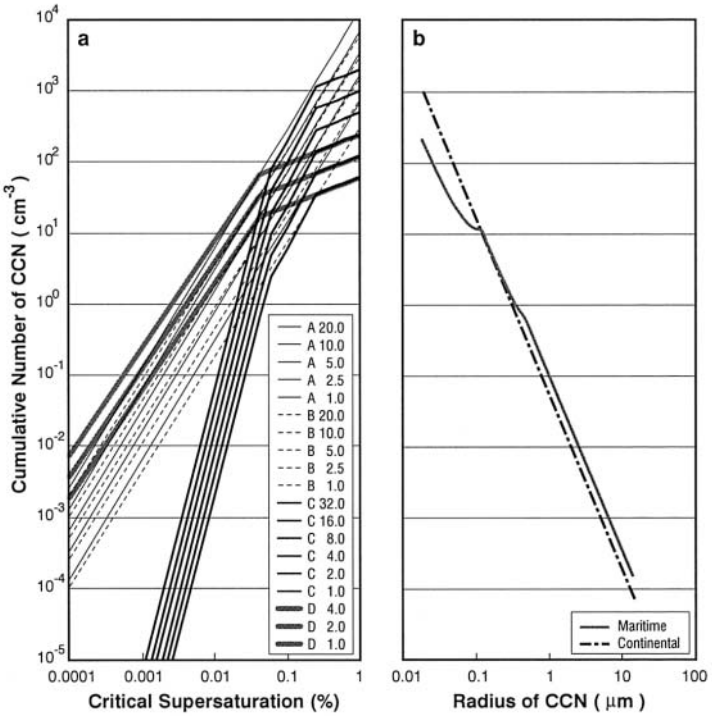

Fig. 2. (a) Supersaturation spectrum of CCN used as initial conditions. Four types of CCN spectrum shape are expressed by A, B, C, and D. The numbers following A, B, C, and D are the ratios of concentration to A1.0, B1.0, C1.0, and D1.0, respectively. (b) Size distribution of the continental CCN (transformed from A5.0 with the assumption that the constituent is $(NH_4)_2SO_4$) and maritime CCN assumed in this study.

Cloud layer was divided into several 50-m-thick sub-layers, and single-scattering properties (e.g., optical thickness, single-scattering albedo, and phase function) of each sub-layer were assumed homogeneous. The single-scattering properties of water-phase droplets were calculated from the size distribution of the cloud droplets in each sub-layer, using Mie theory. Rayleigh scattering was included, but no aerosol particles were assumed in any sub-layer, as the optical depth of aerosols is much smaller than that of cloud droplets. The complex refractive indices were taken from Hale and Querry (1973) for 0.2–1.8 μm, and Downing and Williams (1975) for 2.0–4.0 μm.

Wavelengths from 0.2 to 4.0 μm were divided into 80 sub-bands, and the spectral solar flux for each sub-band was calculated and then integrated for the entire spectral region. Ground surface reflectance was assumed to be zero in order to focus on the optical properties of the cloud layer only. Upward and downward fluxes at the top and bottom of the cloud layer were calculated. Reflectance is defined as the ratio of upward flux to downward flux at the top of the cloud.

4. Results

4.1 Simulated microstructure of a cloud

If the vertical structure of the atmosphere is the same and air parcels ascend adiabatically, all profiles of the liquid water content within the clouds are the same and the LWP depends on cloud depth only. Under a fixed LWP, differences in the optical properties are caused by differences in the number of droplets, determined by the vertical profiles of supersaturation in the cloud and CCN spectrum.

The vertical profiles of supersaturation for the three cases with $LWP = 100$ g m^{-2}, which is equivalent to a cloud depth of 300 m, are shown in Fig. 3. Supersaturation is maximal within 20 m above the cloud base. The larger ascent velocity causes the supersaturation

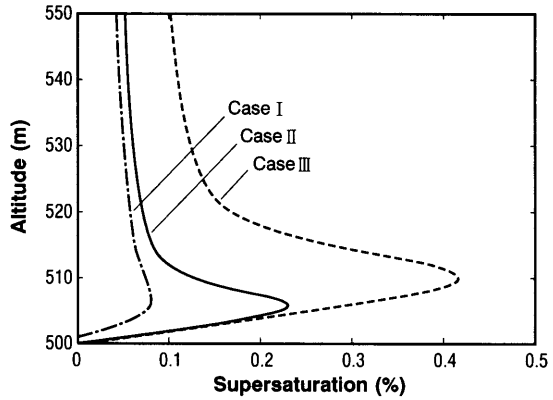

Fig. 3. Vertical profiles of relative humidity in cases I, II, and III for 300 m cloud depth.
Case I: CCN is A20.0 in Fig. 2a. The ascent velocity at the cloud base is 0.06 m s^{-1}.
Case II: CCN is A1.0 in Fig. 2a. The ascent velocity at the cloud base is 0.06 m s^{-1}.
Case III: CCN is A1.0 in Fig. 2a. The ascent velocity at the cloud base is 0.24 m s^{-1}.

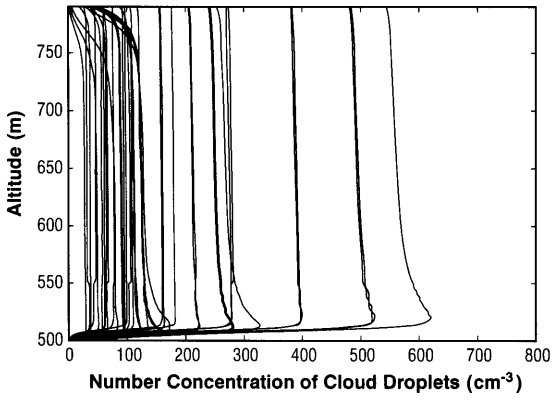

Fig. 4. Vertical evolution of the number of cloud droplets for 300 m cloud depth. The cloud base is at 500 m.

peak to be higher and wider (compare case II (CCN spectrum is A1.0 in Fig. 2a, the ascent at the cloud base is 0.06 m s^{-1}) and case III (A1.0, 0.24 m s^{-1})). Larger CCN concentrations reduce the maximum supersaturation, but do not make the peak narrower (compare case I (A20.0, 0.06 m s^{-1}) and case II (A1.0, 0.06 m s^{-1})). The width and maximum value of the supersaturation peak control the minimum radius of activated CCN, and this radius, together with the CCN size distribution, determines the final number of cloud droplets.

Figure 4 shows the vertical evolution of the number of cloud droplets for 57 cases (combining three vertical profiles of updraft velocity and 19 CCN spectra) with $LWP = 100$ g m^{-2} (cloud depth is 300 m). In this study, the difference in radius between wet CCN which can not be activated and activated CCN which grow to droplets is very clear. Usually 1 μm in droplet radius can be used as the division of the criteria. For some cases, the number of droplets decreases after reaching its maximum value near the cloud base. This shows that even after growing beyond their critical radii, some CCN revert to being inactivated once supersaturation reaches its maximum value. The number of droplets is almost constant in the middle and upper layers of the cloud. Thus, the number of cloud droplets at 100 m above the cloud base is used as the representative value hereafter (N_d).

Some cases in which the number of cloud droplets decreases rapidly near the cloud top correspond to cases with weak ascent and few small particle CCN, but many large and giant particle CCN (ex. D1.0, D2.0 and D4.0 in Fig. 2). For these cases, the number of raindrops produced by coalescence is too great to be neglected, and the consumption of cloud droplets is therefore overestimated as this model ignores the fall-out of raindrops. Therefore, the number of droplets in these cases cannot be estimated precisely. However, the formation of raindrops occurs at levels higher than 250 m above cloud base. For all cases with a 200- or 250-m cloud depth, and for almost all cases with a 300-m cloud depth, the number of cloud droplets at the middle altitude of the cloud is likely to be the representative value.

Figure 5 shows examples of the vertical evolution of droplet size distribution for the case $LWP = 100$ g m^{-2}. This evolution is expressed in Fig. 5a as dN/dR in the case of large concentrations of CCN (A20.0 in Fig. 2a) and a large ascent velocity (**a** in Fig. 1). Many cloud droplets are produced in this case (591 cm^{-3} near the cloud base). Similarly, Fig. 5b shows the evolution of the cloud droplet size distribution at smaller concentrations of CCN (A1.0 in Fig.

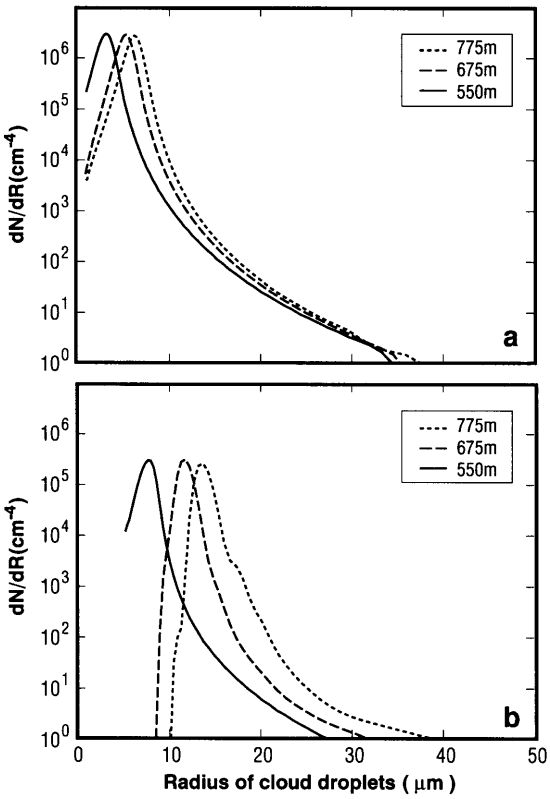

Fig. 5. Vertical evolution of the cloud droplets' size distribution for the case of $LWP = 100$ g m^{-2}. The cloud base is at 500 m. (a) CCN spectrum is A20.0 in Fig. 2a. The ascent velocity profile is **a** in Fig. 1. (b) The CCN spectrum is A1.0 in Fig. 2a. The ascent velocity profile is **c** in Fig. 1.

2a) and weaker ascent velocity (**c** in Fig. 1). Fewer cloud droplets are produced in this case (57.1 cm^{-3} near the cloud base). Low concentrations of CCN and weak ascent velocity lead to fewer cloud droplets, but with a relatively large mean or effective radius. These cloud droplets can then effectively produce large droplets by coalescence. On the other hand, in the case with the higher number concentration of cloud droplets, condensational growth rate is smaller because of the lower supersaturation. Therefore the fewer droplets can start to grow by coalescence.

The number concentration N_d and effective radius R_e of cloud droplets at each altitude in Fig. 5 are listed in Table 2, which shows that CCN and ascent velocity significantly affect the

Table 2. Parameters of cloud droplet size distribution in Fig. 5.

Size distribution	Altitude (m)	Cloud droplet number concentration (cm^{-3})	Cloud droplet effective radius (μm)
a	775	549	6.57
	675	559	5.65
	550	591	3.80
b	775	50.9	14.9
	675	56.2	11.9
	550	57.1	7.82

Cloud base is at 500 m.
Cloud top is at 800 m.

number concentration, effective radius and size distribution of cloud droplets. The change with altitude is much larger for the effective radius than for cloud droplet number concentration. Therefore, the cloud droplet number concentration is a better parameter than the effective radius for calculating the optical properties of clouds. Stephens (1978) proposed an approximate equation for the optical thickness as a function of LWP and effective radius, under the assumption that the drop-size distribution is vertically uniform. However, effective radius changes significantly with altitude, as shown in Table 2. The approximate equation of the optical thickness is better as a function of LWP and N_d than as a function of LWP and R_e.

4.2 *The effect of anthropogenic and giant particle CCN on the optical properties of clouds*

The effect of anthropogenic and giant particle CCN on the optical properties of layer clouds is highlighted in Fig. 6. Figure 6a shows the relationship between the optical thickness of cloud and the number concentration of small particle CCN ($r < 0.1$ μm) added as pollution to continental CCN (shown in Fig. 2b) for three updraft velocities (**g**, **h**, and **i** in Fig. 1; their velocities at the cloud base are 0.24 m s^{-1}, 0.12 m s^{-1} and 0.06 m s^{-1} respectively). The CCN are composed of $(NH_4)_2SO_4$. Figure 6b shows the same relationship as Fig. 6a, but for small particle CCN added to maritime CCN. For maritime CCN, the concentration of small particles is smaller and the concentration of giant par-

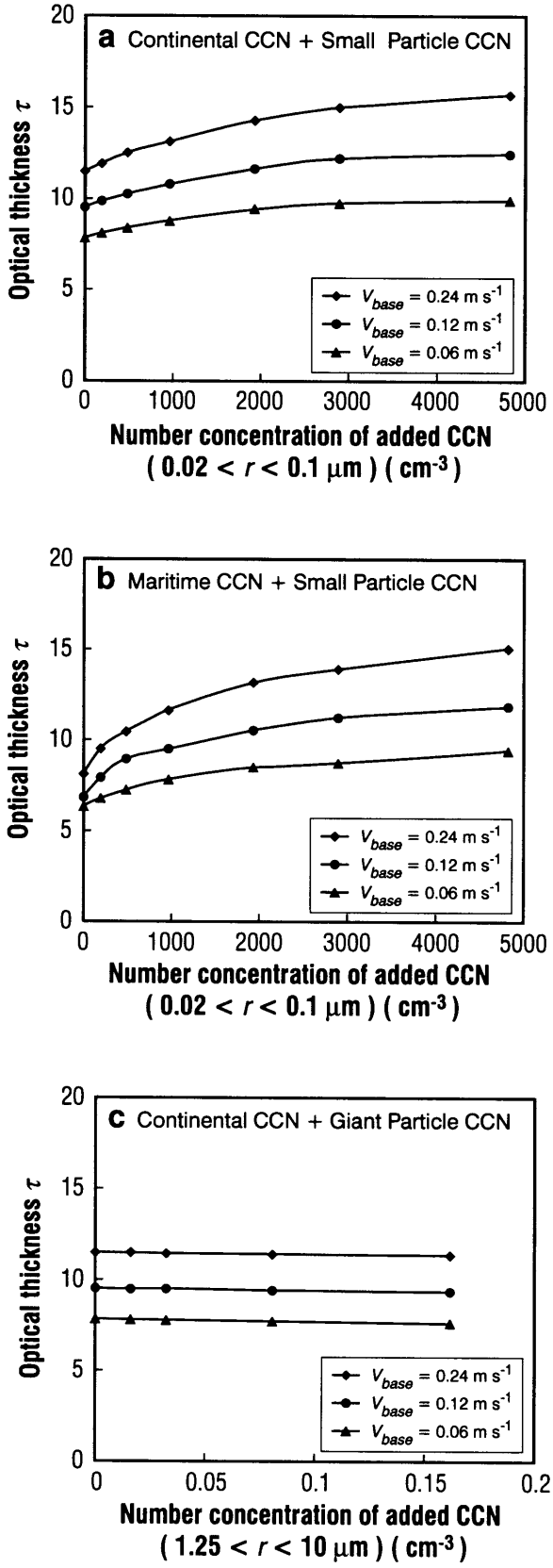

ticles ($r > 1.0$ μm) is larger than it is for continental CCN, as shown in Fig. 2b. The optical thickness changes caused by the addition of small particle CCN are more pronounced for maritime air masses than for continental air masses, especially in areas of rapid ascent. This is because the sensitivity of cloud droplet number concentration to CCN concentration is greater for a smaller number concentration of CCN, and for a faster ascent, as shown later.

Figure 6c shows the relationship between the optical thickness of cloud and the concentration of giant particle CCN, added to the continental CCN. Only a slight effect on optical thickness is noted. The addition of giant particle CCN minimally decreases the cloud droplet concentration, even in continental air masses, where the giant particle concentration is smaller than in maritime air masses.

To estimate the indirect radiative forcing of added CCN, the relationship between the reflectance of cloud for solar radiation (zenith angle θ_s is 60 degrees) and the number concentration of CCN added as pollution, is shown in Fig. 7 for the same cases as Fig. 6. The addition of CCN increases the reflectance of nonprecipitating clouds, and this effect is greater in a maritime air mass than a continental air mass. For a large concentration of CCN, the reflectance is saturated. This suggests that indirect radiative forcing by anthropogenic aerosols enhances cooling, when changes in the "dirtiness" of a cloud and cloud amount are neglected, because absorption is not sensitive to CCN concentration. However, the radiative forcing from anthropogenic CCN would not be

Fig. 6. (a) Relationship between the optical thickness of cloud and the number concentration of small particle CCN ($r < 0.1$ μm) added as pollution to continental CCN (shown in Fig. 2b) for three updraft velocities (**g**, **h**, and **i** in Fig. 1; their velocities at the cloud base are 0.24 m s^{-1}, 0.12 m s^{-1}, and 0.06 m s^{-1} respectively). Cloud depth is 200 m ($LWP = 44$ g m^{-2}). The CCN are composed of $(NH_4)_2SO_4$. (b) The same as (a), but for small particle CCN added to maritime CCN. (c) The same as (a), but for giant particle CCN added to the continental CCN.

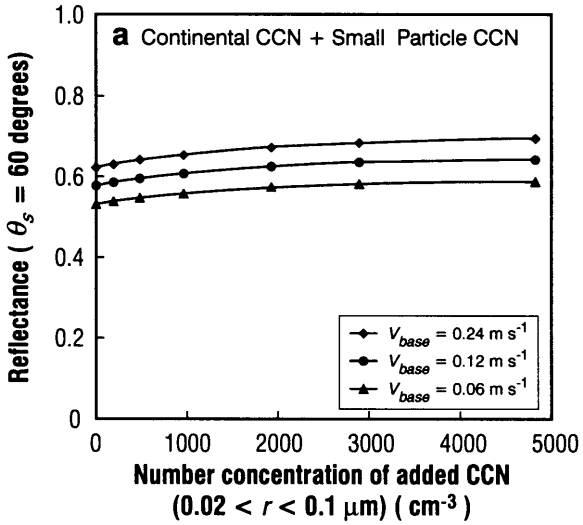

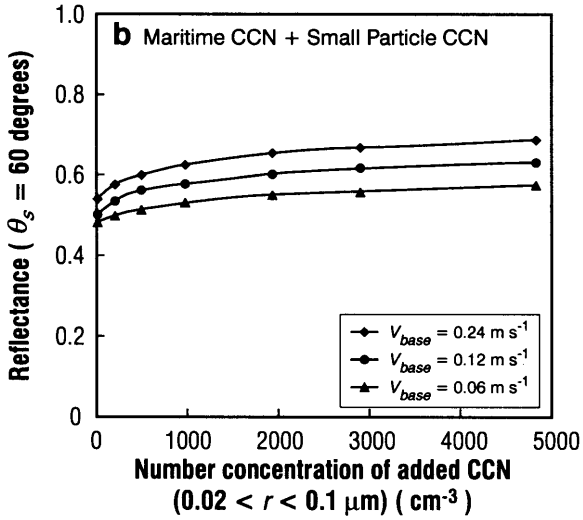

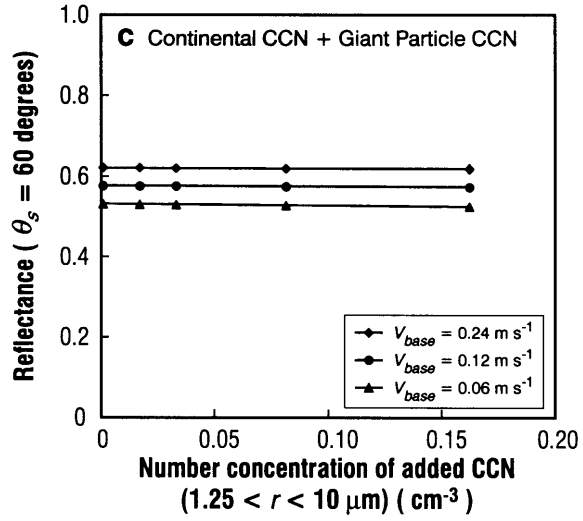

Fig. 7. Relationship between cloud reflectance and the concentration of added CCN for the same cases as Fig. 6. (a) Small particle CCN are added to continental CCN. (b) Small particle CCN are added to maritime CCN. (c) Giant particle CCN are added to continental CCN.

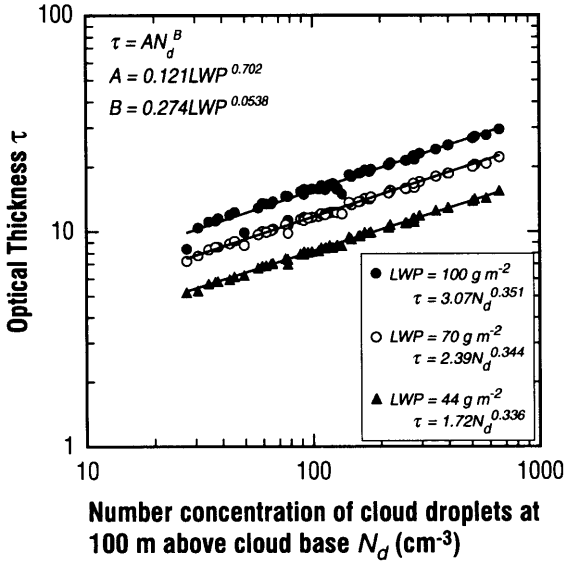

Fig. 8. Relationship between the optical thickness (τ) of a cloud and cloud droplet concentration at 100 m above cloud base (N_d) for the cases with $LWP = 100$, 70 and 44 g m^{-2}. For each LWP, there are 57 cases, which represent combinations of the three vertical profiles of updraft velocity, and 19 CCN spectra.

dominant in an air mass rich in CCN. On the other hand, the effect of an addition of giant particle CCN on the reflectance is small.

As shown here, the effect of CCN on the optical properties of clouds depends on air mass. To estimate this effect quantitatively, the parameterization is developed in the following sections.

4.3 *Relationship between cloud optical thickness, effective radius and droplet concentration*

Figure 8 shows the relationship between the optical thickness of a cloud (τ), and the concentration of cloud droplets at 100 m

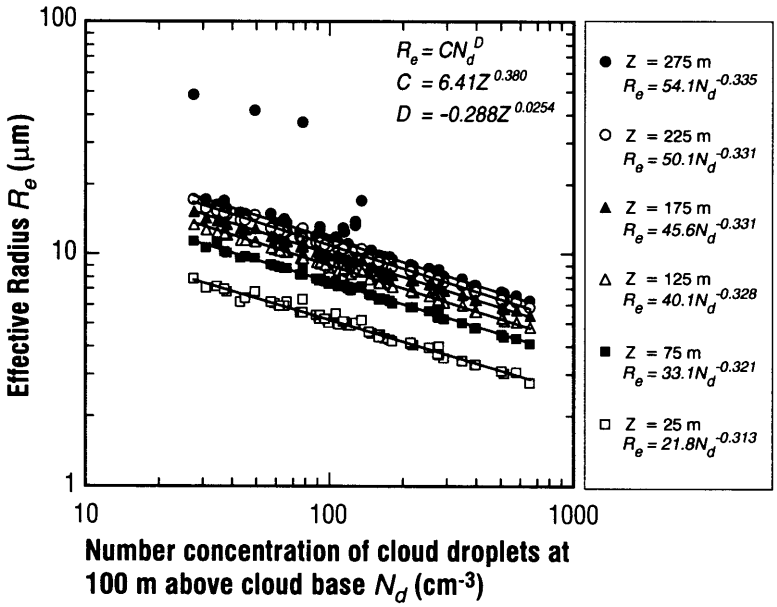

Fig. 9. Relationship between the effective radius of cloud droplets (R_e) at each level in a cloud and the concentration of cloud droplets at 100 m above the cloud base (N_d) for the cases with $LWP = 100$ g m^{-2}, $LWP = 70$ g m^{-2}, and $LWP = 44$ g m^{-2}.

above the cloud base (N_d), for the cases of $LWP = 100$ g m^{-2} (cloud depth is 300 m), $LWP = 70$ g m^{-2} (cloud depth is 250 m) and $LWP = 44$ g m^{-2} (cloud depth is 200 m). There are 57 cases for each LWP, which represent combinations of the three vertical profiles of updraft velocity and 19 CCN spectra. Almost all points are on one line for each LWP. The points that vary from the line in the case of $LWP = 100$ g m^{-2} correspond to the cases with weak ascent and few small particle CCN, but with many large and giant particle CCN. For these cases, effective radii are overestimated near the cloud top, because this model ignores the fall-out of raindrops, as mentioned previously. However, these points do not stand out in the case of thinner clouds. Drizzle does not accompany these thinner clouds.

It was found that the optical thickness of non-precipitating layer clouds can be estimated by the LWP and the number of cloud droplets at the middle altitude in the cloud, despite differences in the shape of the cloud droplets' size distribution. The approximate equation of the optical thickness is expressed as a function of the number of cloud droplets (N_d) at the middle altitude in the cloud as follows.

$$\tau = AN_d^B. \quad (1)$$

The coefficients in the equation, A and B, are functions of the LWP.

$$A = 0.121LWP^{0.702},$$

$$B = 0.274LWP^{0.05}.$$

Brenguiter et al. (2000) showed that optical thickness is proportional to $N_d^{1/3}$ and $LWP^{5/6}$. This roughly accords with our results (as the dependence of B on LWP is small, B is roughly 0.34, and τ is roughly proportional to $LWP^{0.7}$).

Figure 9 shows the relationship between the effective radius of cloud droplets (R_e) at each level in a cloud and the concentration of cloud droplets at 100 m above the cloud base (N_d), for the cases of $LWP = 100$ g m^{-2}, $LWP = 70$ g m^{-2}, and $LWP = 44$ g m^{-2}. The effective radius at each altitude in the cloud is expressed by the following approximate equation.

$$R_e = CN_d^D. \quad (2)$$

The coefficients in the equation, C and D, are functions of the LWP.

$$C = 6.41Z^{0.380},$$

$$D = -0.288Z^{0.0254},$$

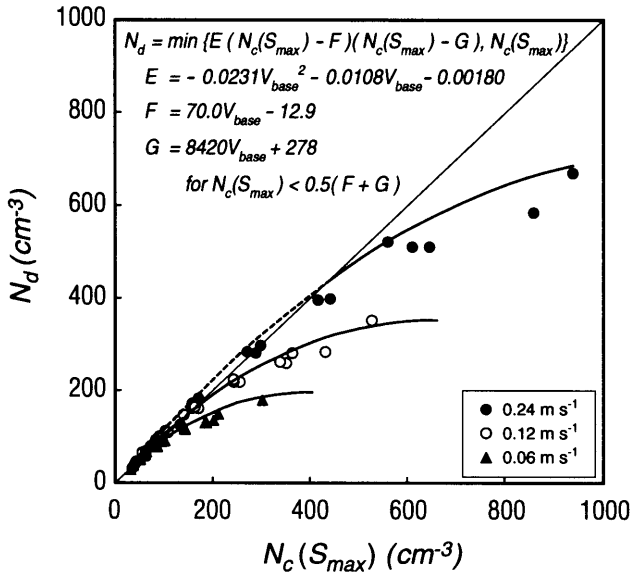

Fig. 10. Relationship between the concentration of cloud droplets at 100 m above cloud base (N_d) and the cumulative concentration of CCN for which critical supersaturation is lower than the simulated maximum supersaturation ($N_c(S_{max})$) for three updraft velocities at the cloud base ($V_{base} = 0.24$, 0.12, and 0.06 m s^{-1}).

where Z is an altitude above cloud base. The points that vary from the line for $Z = 275$ m (near the cloud top for thick cloud) correspond to cases with drizzle, as mentioned previously. This suggests that the optical properties of thicker clouds that cause drizzle cannot be estimated by a simple function, as has been noted in Feingold et al. (1997). For non-precipitating clouds, however, this error is small.

4.4 *Predicting the concentration of cloud droplets from CCN observations*

As shown above, predicting the concentration of cloud droplets is useful for predicting the optical properties of thin layer clouds. Figure 10 shows the relationship between the number of cloud droplets at 100 m above the cloud base (N_d) and the cumulative number of CCN ($N_c(S_{max})$) for three updraft velocities near the cloud base (V_{base}). Here, $N_c(S)$ means the cumulative number concentration of CCN that can be activated under the constant supersaturation S (meaning that their critical supersaturation values are smaller than S). S_{max} is the maximum supersaturation realized near the cloud base. Usually, N_d is assumed to be equal to $N_c(S_{max})$. Note that $N_c(S_{max})$ is not always equal to the concentration of cloud droplets N_d; N_d is smaller than $N_c(S_{max})$ when $N_c(S_{max})$ is large or V_{base} is small. The reduction is larger for a case with smaller updraft and larger $N_c(S_{max})$. Supersaturation decreases more rapidly for the smaller updraft case, as shown in Fig. 3 (compare cases II and III), and growth by condensation is slower because of the smaller supersaturation in the case with larger $N_c(S_{max})$, as suggested in Fig. 3 (compare cases I and II). More CCN with critical supersaturation near S_{max} become inactivated after they initially grow beyond their critical radii because of the reduction in supersaturation. Figure 10 includes all the CCN size distributions shown in Fig. 2a; therefore, these relationships are general. The assumption that N_d is equal to $N_c(S_{max})$ is possible for the cases with N_d smaller than about 80 cm^{-3} (when V_{base} is 0.06 m s^{-1}), N_d smaller than about 160 cm^{-3} (when V_{base} is 0.12 m s^{-1}) and N_d smaller than about 400 cm^{-3} (when V_{base} is 0.24 m s^{-1}).

If $N_c(S_{max})$ and the ascent velocities near the cloud base V_{base} are known, N_d can be estimated using the following equations:

$$\begin{aligned} N_d &= min\{E(N_c(S_{max}) - F) \\ &\quad \times (N_c(S_{max}) - G), N_c(S_{max})\}; \\ E &= -0.0231V_{base}^2 - 0.0108V_{base} - 0.00180; \\ F &= 70.0V_{base} - 12.9; \quad \text{and,} \\ G &= 8420V_{base} + 278. \end{aligned} \tag{3}$$

These are applicable to $N_c(S_{max}) < 0.5(F + G)$. At $N_c(S_{max}) = 0.5(F + G)$, N_d is almost saturated as $N_d = -0.25E(G - F)^2$.

$N_c(S_{max})$ can be estimated from S_{max} and the supersaturation spectrum of CCN. Figure 11 shows the relationships between the simulated maximum supersaturation S_{max} and $N_c(0.075\%)$ for three updraft velocities near the cloud base, V_{base}. A critical supersaturation of 0.075% means that the dry nucleus radius is about 0.069 μm for NaCl, or about 0.090 μm for $(NH_4)_2SO_4$. This means that $N_c(0.075\%)$ is the cumulative number of CCN larger than 0.069 μm in radius if the constituent of CCN is NaCl. This figure shows that S_{max} can be ap-

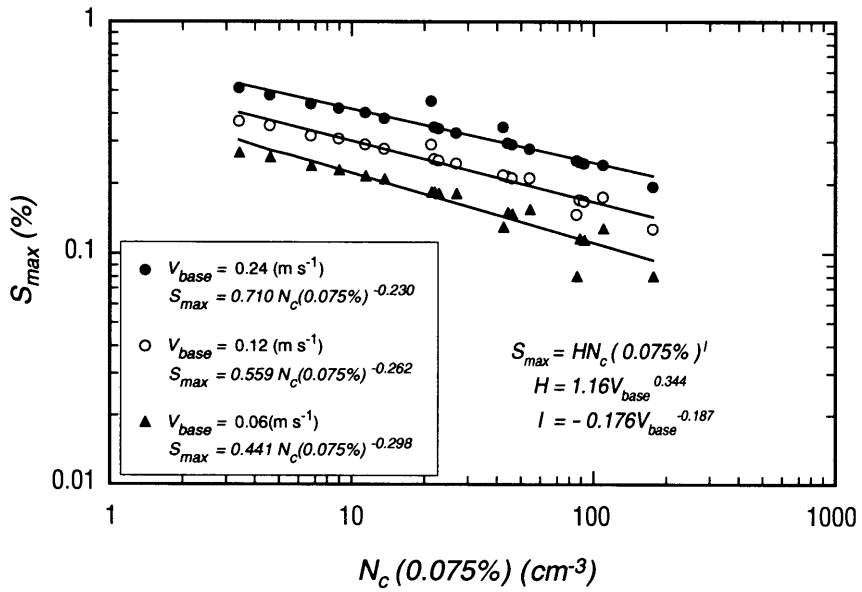

Fig. 11. Relationship between S_{max} and the cumulative concentration of CCN for which the critical supersaturation is lower than 0.075% ($N_c(0.075\%)$) for three updraft velocities at the cloud base ($V_{base} = 0.24$, 0.12, and 0.06 m s^{-1}).

proximated by $N_c(0.075\%)$ when the cloud base updraft is given. Basically, we can make the same approximation using $N_c(S)$ as that using $N_c(0.075\%)$. However, the deviation of simulated values from approximated values is minimum at $S = 0.075\%$ for the range of V_{base} assumed here.

The cumulative CCN concentrations, $N_c(0.075\%)$, can predict the approximate value of S_{max}, and values of $N_c(S_{max})$ can be used to predict the concentration of cloud droplets, if the updraft velocity near the cloud base is known.

$$S_{max} = HN_c(0.075\%)^I. \tag{4}$$

Where,

$$H = 1.16V_{base}^{0.344},$$

$$I = -0.176V_{base}^{-0.187}.$$

If such an accurate estimation is not needed, a rough approximation of N_d without using the maximum supersaturation can be used as follows. Figure 12 shows the relationship between cloud droplet number concentration N_d and the cumulative number of CCN at 0.2% supersaturation $N_c(0.2\%)$. Critical supersaturation of 0.2% corresponds to the radius of 0.036 μm (0.048 μm) for the dry nucleus of NaCl ($(NH_4)_2SO_4$). The approximate equation of N_d is as follows.

$$N_d = J \ln N_c(0.2\%) + K. \tag{5}$$

Where,

$$J = 724V_{base} - 8.07,$$

$$K = -2410V_{base} + 70.4.$$

As shown in Fig. 12, this equation can not be used for small $N_c(0.2\%)$. Expediently the following equation is applied for $N_c(0.2\%) < 50$ cm^{-3}.

$$N_d = (0.0782J + 0.02K)N_c(0.2\%); \tag{5}'$$

Basically, the same approximation using $N_c(S)$ can be made as that using $N_c(0.2\%)$. However, the deviation of simulated values from approximated values is minimum at $S = 0.2\%$ for the range of V_{base} assumed here. This equation can estimate cloud droplet number concentration directly from the cumulative number of CCN. However, this is less accurate than the preceding parameterization.

4.5 Retrieval method to predict the CCN number concentration

The rough estimation of N_d as a function of the cumulative number of CCN in Fig. 12 enables us to retrieve CCN number concentration

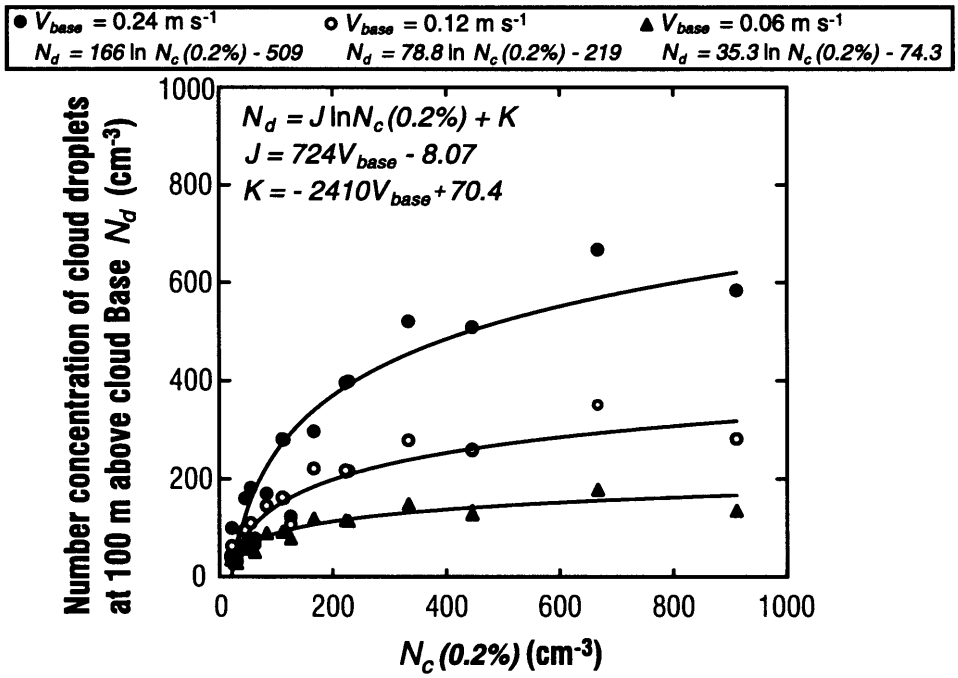

Fig. 12. Relationship between cloud droplet number concentration at 100 m above cloud base N_d and the cumulative number of CCN at 0.2% supersaturation $N_c(0.2\%)$. The ascent velocity at the cloud base is 0.24, 0.12 or 0.06 m s^{-1}.

from the observational data of the optical properties of clouds. Equations (5) and (5)′ are rewritten as follows.

$$N_c(0.2\%) = \exp\{(N_d - K)/J\}, \quad \text{for } N_d > 3.91J + K,$$
$$N_c(0.2\%) = (0.0782J + 0.02K)^{-1}N_d, \quad \text{for } N_d \leqq 3.91J + K. \tag{6}$$

N_d is obtained from the independent remote sensing data of non-precipitating thin layer clouds by using the approximate equation derived in this study (equation (1)). The independent data are optical thickness that can be retrieved with visible wave length sensor, and the LWP that can be retrieved with micro-wave radiometer.

5. Verification of the new parameterization and retrieval method

5.1 Comparison with simulations

Figure 13 shows the relationship between the cloud droplet number concentration at 100 m above the cloud base, as simulated by our

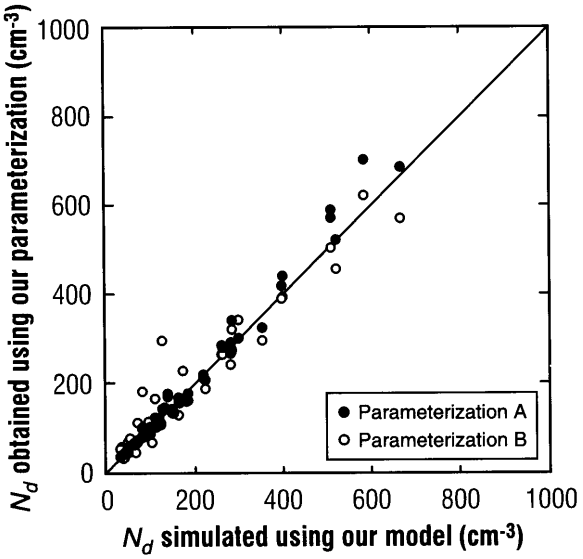

Fig. 13. Relationship between the cloud droplet number concentration at 100 m above cloud base N_d simulated by our model and that obtained by using the parameterization developed in this study. Parameterization A uses equations (3) and (4); parameterization B uses equation (5) or (5)′.

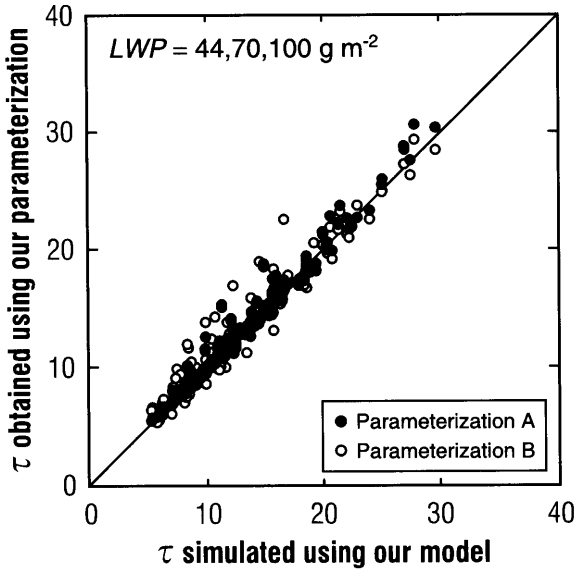

Fig. 14. Relationship between the optical thickness τ simulated by our model and the optical thickness τ obtained by using the parameterization developed in this study. Parameterization A uses equations (1), (3) and (4); parameterization B uses equations (1) and (5) (or (5)′).

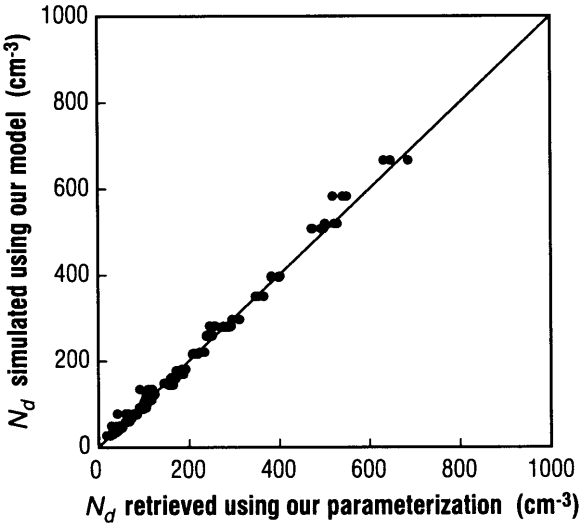

Fig. 15. Relationship between the cloud droplet number concentration at 100 m above cloud base N_d simulated by our model and that retrieved from optical thickness by using equation (1).

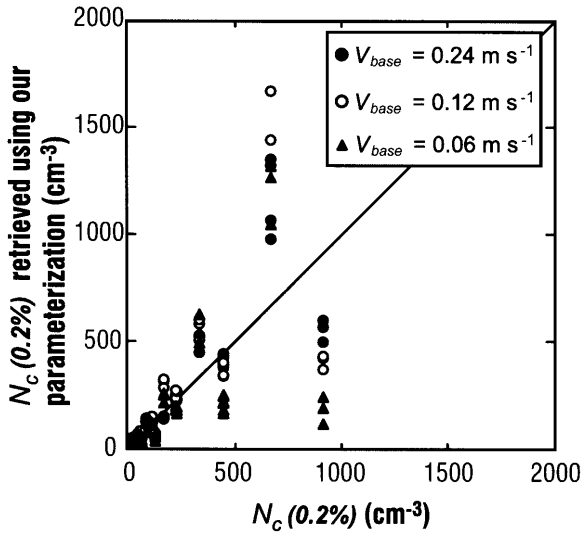

Fig. 16. Relationship between the CCN cumulative number concentration $N_c(0.2\%)$ and that retrieved from optical thickness by using equations (1) and (6).

model, and that obtained by using the parameterization developed in this study. Parameterization A uses equations (3) and (4); parameterization B uses equation (5) or (5)′.

Figure 14 shows the relationship between the optical thickness simulated by the model, and the optical thickness obtained by using the parameterization developed in this study. Parameterization A uses equations (1), (3), and (4); parameterization B uses equations (1) and (5) (or (5)′).

Figures 13 and 14 show that parameterization A can predict the cloud droplet number concentration and the optical thickness very precisely. Parameterization B is less accurate than parameterization A.

Figure 15 shows the relationship between the cloud droplet number concentration at 100 m above the cloud base simulated by our model, and that retrieved from the optical thickness by using equation (1). It shows that equation (1) can retrieve the cloud droplet number concentration accurately.

Figure 16 shows the relationship between the CCN cumulative number concentration $N_c(0.2\%)$, and that retrieved from the optical thickness by using equations (1) and (6). It shows that this method has a large error in

Table 3. Comparison between observation and parameterization.

	Parameter	Polluted air			Clean air		
Observation	$N_c(0.075\%)$ (cm^{-3})	200			6		
	$N_c(0.2\%)$ (cm^{-3})	430			16		
	N_d (cm^{-3})	220			10–35		
	V_{base} (m s^{-1})	0.00 ± 0.29			0.12 ± 0.26		
	Assumed V_{base} (m s^{-1})	0.2	0.1	0.05	0.2	0.1	0.05
Parameterization A	S_{max} (%)	0.19	0.13	0.08	0.44	0.32	0.24
	$N_c(S_{max})$ (cm^{-3})	400	300	210	100	45	22
	N_d (cm^{-3})	351	239	141	100	45	22
Parameterization B	N_d (cm^{-3})	418	219	120	39	26	19

cases with large $N_c(0.2\%)$ or small ascent velocity. In those cases, S_{max} does not reach 0.2% and the correlation between $N_c(0.2\%)$ and N_d is weak, as shown in Fig. 12. This retrieval method is applicable only when the ascent velocity at the cloud base is larger than 0.1 m s^{-1}, and $N_c(0.2\%)$ is smaller than 500 cm^{-3}. However, it is useful to obtain information on a global scale on CCN from the observational data of optical thickness. Conventional retrieval methods offer information, on a predictive basis, on aerosol particles. Information on CCN, as opposed to that on aerosol particles, is important for examining the indirect radiative forcing of CCN.

5.2 Comparison with observations

Hudson and Li (1995) measured the CCN spectrum, cloud droplet number concentration and ascent velocity in mid-Atlantic clean and polluted clouds during the Atlantic Stratocumulus Transition Experiment (ASTEX). They provided the optimum data to verify the application of our parameterization. Some observational data, taken from their measurements, are listed in Table 3. Cloud droplet number concentrations, estimated by using these data and the A or B method of parameterization, developed in this study, are also listed in Table 3. As Hudson and Li noted that the average value of ascent velocity in Table 3 is not very accurate, three values 0.2, 0.1, and 0.05 m s^{-1} are assumed here. Our parameterization reproduces the tendency that the ratio of N_d in polluted air to N_d in clean air is smaller than the ratio of $N_c(0.075\%)$ or $N_c(0.2\%)$ in polluted air to that in clean air. Comparison of these estimated and measured number concentrations of cloud droplets, suggests that ascent velocity near the cloud base might be between about 0.05 and 0.1 m s^{-1}. More quantitative comparison between the parameterizations developed in this study and observations, requires more accurate observational data of ascent velocity, preferably observations coupled with Doppler lidar and/or Doppler cloud radar.

6. Concluding remarks

A method to predict changes in the optical properties of layer clouds, caused by changes in CCN, was proposed using a numerical model, constructed to minimize artificial broadening in the cloud droplet size distribution. The procedure is as follows: When we measure (observe) cumulative CCN concentration, $N_c(0.075\%)$, and ascent velocity at the cloud base, V_{base}, we can predict the approximate value of S_{max}. Using this S_{max}, we can then estimate $N_c(S_{max})$, which in turn is used with V_{base} to predict the concentration of cloud droplets at the middle altitudes of a layer cloud (N_d). For fixed *LWP*, optical thickness τ and effective radius $R_e(Z)$ can be estimated from N_d, unless drizzle is falling from the cloud.

In addition, this study developed an approximation to directly predict N_d using $N_c(0.2\%)$ and V_{base}, although this is less accurate than the preceding parameterization. However, this approximation does not need $N_c(S_{max})$, and it enables retrieval of CCN number concentration from observational data of the optical properties of clouds. It is very useful for obtaining information on CCN number concentration on

a global scale. Conventionally, remote sensing data provide information on aerosol particles, but not on CCN particles. In order to examine the indirect radiative forcing of CCN, information on CCN is required, as opposed to information on aerosol particles.

In addition, the following conclusions are noted:

(1) N_d is smaller than $N_c(S_{max})$. Some CCN with critical supersaturation near S_{max} revert to being inactivated after growing beyond their critical radii, because of a reduction in supersaturation with height. The reduction in concentration is larger for smaller updrafts, and larger $N_c(S_{max})$;
(2) The sensitivity of N_d to the concentration of CCN is greater for stronger updrafts, or smaller CCN concentrations. Thus, N_d and cloud optical properties in air masses with strong updrafts and smaller CCN concentrations, are affected more significantly by introducing anthropogenic CCN; and,
(3) The changes in the optical thickness and reflectance of non-precipitating thin layer clouds caused by the addition of small particle CCN, are more pronounced in maritime air masses than in continental air masses, especially when ascent velocity is high. The addition of giant CCN has only a slight effect on a cloud's optical properties.

Layer cloud optical properties are most sensitive to anthropogenic aerosols in air masses with a relatively small initial CCN concentration, especially in cases with strong updrafts near the cloud base. Therefore, the size distributions of both the background CCN and of the added aerosols that can work as CCN, are important when considering the indirect radiative forcing of anthropogenic aerosols. These results are consistent with ship track observations (Taylor et al. 2000), and long-term global observations using remote sensing (Kawamoto 1999). The addition of anthropogenic aerosols increases the optical thickness of non-precipitating clouds in a clean air mass, but absorption is not sensitive to CCN concentration. This suggests that indirect radiative forcing by anthropogenic aerosols enhances cooling, when changes in the "dirtiness" of a cloud and cloud amount are neglected. However, the radiative forcing from anthropogenic aerosols would not be dominant in an air mass rich in CCN.

The CCN spectrum has been measured over a wide range (0.01–1% supersaturation) (Hudson and Frisbie 1991; Hudson and Li 1995; Hudson and Yum 2001). A microwave radiometer can detect the LWP of a cloud. Ascent velocity in a cloud is not easy to measure, especially for stratus cloud, but it is expected that a Doppler lidar will be able to measure ascent velocity. The combination of remote sensing and in situ measurement make the parameterization developed in this study useful. In addition, global information on CCN could be obtained if Doppler lidar and/or Doppler cloud radar is installed on future satellites, such as EarthCARE (European Space Agency 2001).

This study assumes that the cloud base is at an altitude of 500 m in the U.S. Standard Atmosphere 1976. Since pressure has little affect on droplets' growth by condensation, and the difference in temperature due to the difference in altitude is small, varying the cloud base altitude does not greatly alter the study results in the case of warm clouds. Higher cloud bases lead to a somewhat smaller LWP for a fixed cloud depth. When the air temperature at the cloud base is the lower (it is assumed 284.9 K in this study), the more CCN are activated due to the higher maximum supersaturation, and the smaller LWP is produced. Since the increase in the number concentration of cloud droplets N_d, and the decrease in the LWP, have the opposite effect for the optical thickness τ of clouds, τ becomes slightly decreases. The parameterizations to predict N_d using equations (3) and (4) or that using equation (5) (or (5)′) have the tendency to underestimate N_d, when the cloud base temperature is lower than 284.9 K. The error is about 10% for five-degree cooling. The underestimated N_d and true value of LWP lead to τ underestimated. The error is about 10% for five-degree cooling. If necessary, the model can make the adequate parameterization for the different cloud base temperature, by changing the vertical profile of air temperature. The retrieval method using equation (1) can predict N_d accurately even if the cloud base temperature is different from that in this study. However, the retrieval method to predict $N_c(0.2\%)$ using equation (6), has the tendency to overestimate it when the cloud

base temperature is lower than 284.9 K. Since this method has low accuracy, the error caused by the difference in cloud base temperature is not so important. If necessary, the parametarizations for the extremely different atmosphere from that used here can be developed in the same way.

Acknowledgments

We would like to express our sincere thanks to Dr. Andreas Bott, who kindly furnished the FORTRAN code used for the flux method of stochastic collection, and discussed the scheme with us.

Appendix

The scheme using fixed bins to calculate the time evolution of droplet size distribution caused by condensation growth

Numerical diffusion is a serious problem when fixed bins of droplet radius are used to estimate the time evolution of droplet size distribution caused by condensation. Since numerical diffusion affects the optical properties and precipitation efficiency of clouds, this scheme is developed with a special eye towards avoiding numerical diffusion, and keeping droplet concentrations positive.

We followed the advection scheme developed by Bott (1989). The size distribution is expressed as

$$\varphi = \frac{dn}{d\ln r} = \frac{dn}{dy}. \tag{A1}$$

In a flow field, the continuity equation describing the transport of a non-diffusive quantity is given by

$$\frac{d\varphi}{dt} = \frac{\partial}{\partial y}\left(\frac{dy}{dt}\varphi\right). \tag{A2}$$

By assuming constant bin spacing Δy and time increments Δt, the finite difference flux form of equation (A2) is expressed as

$$\varphi_i^{n+1} = \varphi_i^n - \frac{\Delta t}{\Delta y}(F_{i+1/2}^n - F_{i-1/2}^n), \tag{A3}$$

where φ_i^n is the value of $\varphi(y = y_i, t = t_n)$, and $F_{i+1/2}^n$, $F_{i-1/2}^n$ are the φ-fluxes through the right and left boundary of the bin, respectively.

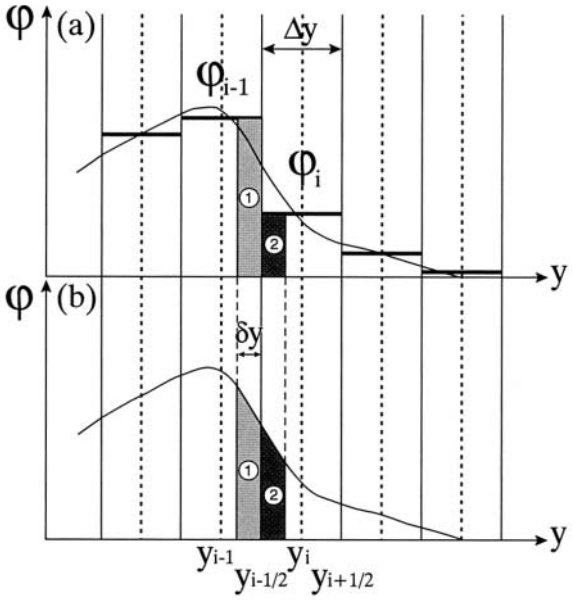

Fig. A1. Relationship between φ and $F_{i-1/2}^n \Delta t$. (a) φ is assumed constant in each bin. (b) The distribution of φ is considered in each bin.

If the constant values of φ in each bin is assumed, as in Fig. A1a, $F_{i-1/2}^n \Delta t$ is equivalent to the shadowed area 1 (/ area 2) for the case of positive (/ negative) $\frac{dy}{dt}$ at $y_{i-1/2}$. This assumption, however, generates large numerical diffusion, so the distribution of φ in each bin considered, as in Fig. A1b. In Fig. A1b, $F_{i-1/2}^n \Delta t$ is equivalent to the shadowed area 1 (/ area 2) in the case of positive (/ negative) $\frac{dy}{dt}$ at $y_{i-1/2}$.

The two straight lines joined at the center of the bin represent φ in each bin.

$$\varphi_i(y) = \left[\varphi_i + \frac{\varphi_{i+1} - \varphi_i}{\Delta y}(y - y_i)\right]\alpha_i \quad \text{for } y_i < y < y_{i+1/2}, \tag{A4}$$

$$\varphi_i(y) = \left[\varphi_i + \frac{\varphi_{i-1} - \varphi_i}{\Delta y}(y - y_i)\right]\alpha_i \quad \text{for } y_{i-1/2} < y < y_i, \tag{A5}$$

α_i is the correction coefficient to guarantee

$$\int_{y_{i-1/2}}^{y_{i+1/2}} \varphi_i(y)\, dy = \varphi_i \Delta y. \tag{A6}$$

In this scheme, Δt is chosen to satisfy the condition

$$\delta y = \left(\frac{dy}{dt}\right)\Delta t < \frac{\Delta y}{2}. \tag{A7}$$

Now, $F^n_{i-1/2}\Delta t$ is expressed as

$$\left(\frac{dy}{dt}\right)_{y_{i-1/2}} > 0;$$

$$\begin{aligned} F^n_{i-1/2}\Delta t &= \int_{y_{i-1/2}-\delta y}^{y_{i-1/2}} \varphi_{i-1}(y)\,dy \\ &= \int_{1/2-(\delta y)/(\Delta y)}^{1/2} (A_0 + A_1 y')\Delta y\,dy' \\ &= \left(A_0 + \frac{A_1}{2}\right)\delta y - \frac{A_1}{2\Delta y}\delta y^2, \end{aligned} \tag{A8}$$

where

$$y' = \frac{y - y_{i-1}}{\Delta y}. \tag{A9}$$

$$A_0 = \alpha_{i-1}\varphi_{i-1}, \tag{A10}$$

$$A_1 = \alpha_{i-1}(\varphi_i - \varphi_{i-1}). \tag{A11}$$

In the same way,

$$\left(\frac{dy}{dt}\right)_{y_{i-1/2}} < 0;$$

$$\begin{aligned} F^n_{i-1/2}\Delta t &= -\int_{y_{i-1/2}}^{y_{i-1/2}+\delta y} \varphi_i(y)\,dy \\ &= -\int_{-1/2}^{-1/2+(\delta y)/(\Delta y)} (A_0 + A_1 y')\Delta y\,dy' \\ &= \left(A_0 - \frac{A_1}{2}\right)\delta y - \frac{A_1}{2\Delta y}\delta y^2, \end{aligned} \tag{A12}$$

where,

$$y' = \frac{y - y_i}{\Delta y}. \tag{A13}$$

$$A_0 = \alpha_i\varphi_i, \tag{A14}$$

$$A_1 = \alpha_i(\varphi_i - \varphi_{i-1}). \tag{A15}$$

We tested the validity of this technique (hereafter, the DL-method, where DL represents the dual-linear line that approximates φ) for estimating droplet growth by condensation via the series of numerical experiments listed in Table A1. Two air parcels (parcel L and par-

Table A1. List of numerical experiments performed to confirm the validity of the DL-method.

	500–550 m Activation + Condensation	550–650 m Condensation	650–775 m Condensation + Coalescence
Parcel L	Lagrangian	Lagrangian	DL-method + Bott's (1998) method
Parcel D	Lagrangian	DL-method	DL-method + Bott's (1998) method

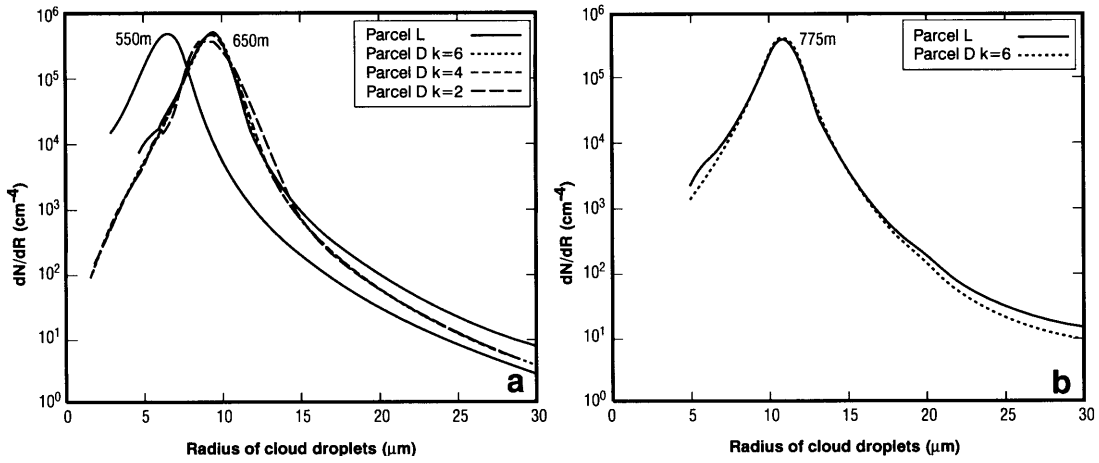

Fig. A2. (a) Size distributions of cloud droplets in parcels L and D ($k = 2$, 4, and 6) at altitudes of 550 and 650 m. (b) Size distributions of cloud droplets in parcels L and D ($k = 6$) at an altitude of 775 m.

cel D) started ascent from a 500-m cloud base. As both parcels rose from 500 m to 550 m, CCN activation and the change of the cloud droplet size distribution with time were calculated using the Lagrangian framework discussed in Section 2.3.a, and coalescence was ignored. In parcel L, condensation-forced changes in the droplet size distribution from 550 to 650 m were calculated using the same Lagrangian formulation as was used from 500 to 550 m. For parcel D, however, the changes in the droplet size distribution from 550 to 650 m were calculated in a Eulerian framework using the DL-method, ignoring coalescence. Figure A2a shows the distributions of cloud droplet size in parcels L and D ($k = 2$, 4 and 6) at altitudes of 550 and 650 m for the case with CCN spectrum A5.0 in Fig. 2a, and ascent velocity **c** in Fig. 1. At 550 m, the four size distributions are the same. As shown in Fig. A2a, for $r < 13$ μm and for $k = 6$, the results from the DL-method give a size distribution consistent with that calculated using the Lagrangian framework. Larger droplets have higher molarity, so in Parcel D their growth rates are underestimated because the solute effect is ignored in calculations using the DL-method. This underestimation occurs only in limited regions of very low concentration, and the difference will not change the optical properties of the cloud unless the efficiency of production of large drops by coalescence is affected.

To understand the effect on the growth rate of underestimation of large drops in parcel D from 650 to 775 m, we calculated the time evolution of cloud droplet size distribution caused by *condensation* using the DL-method, and that caused by *coalescence* using Bott's (1998) method for both parcels. As shown in Fig. A2b, the difference in droplet size distribution between parcel L and D at 775 m ($k = 6$) is small. Production of large drops by the coalescence of major droplets dominates that by the coalescence of drops that have an underestimated condensational growth rate. Therefore, we conclude that this model is effective for estimating the rate of change of cloud droplets' size distribution caused by condensation and coalescence.

References

Brenguier, J.L., H. Pawlowska, L. Schuller, R. Preusker, J. Fischer and Y. Fouquart, 2000: Radiative properties of boundary layer clouds: Effective radius versus number concentration. *J. Atmos. Sci*., **57**, 803–821.

Bott, A., 1989: A positive definite advection scheme obtained by nonlinear renormalization of the advective fluxes. *Mon. Wea. Rev*., **117**, 1006–1015.

———, 1998: A flux method for the numerical solution of the stochastic collection equation. *J. Atmos. Sci*., **55**, 2284–2293.

Chen, J.P. and D. Lamb, 1994: Simulation of cloud microphysics and chemical processes using a multicomponent framework. Part I Description of the microphysical model. *J. Atmos. Sci*., **51**, 2613–2630.

——— and ———, 1999: Simulation of cloud microphysics and chemical processes using a multicomponent framework. Part II Microphysical evolution of a wintertime orographic cloud. *J. Atmos. Sci*., **56**, 2293–2312.

Chuang, P.Y., R.J. Charlson and J.H. Seinfeld, 1997: Kinetic limitations on droplet formation in clouds. *Nature*, **390**, 594–596.

Cooper, W.A., R.T. Bruintjes and G.K. Mather, 1997: Calculations pertaining to hygroscopic seeding with flares. *J. Appl. Meteor*., **36**, 1449–1469.

Downing, H.D. and D. Williams, 1975: Optical constant of water in the infrared. *J. Geophys. Res*., **80**, 1656–1661.

European Space Agency, 2001: *EarthCARE-Earth Clouds*, Aerosols and Radiation Explorer, ESA SP-1257(1), 130pp.

Feingold, G., R. Bores, B. Stevens and W.R. Cotton, 1997: A modeling study of the effect of drizzle on cloud optical depth and susceptibility. *J. Geophys. Res*., **102**, D12, 13527–13534.

Fitzgerald, J.W., 1974: Effect of aerosol composition on cloud droplet size distribution: A numerical study. *J. Atmos. Sci*., **31**, 1358–1367.

Fouquart, Y., J.C. Buriez, M. Herman and R.S. Kandel, 1990: The influence of clouds on radiation: A climate-modeling perspective. *Rev. Geophys*., **28**, 145–166.

Hall, W.D., 1980: A detailed microphysical model within a two-dimensional dynamic framework: Model description and preliminary results. *J. Atmos. Sci*., **37**, 2486–2507.

Hale, G.M. and M.R. Querry, 1973: Optical constant of water in the 200-nm to 200-μm wavelength region. *Applied Optics*, **12**, 555–563.

Higurashi, A., T. Nakajima, R. Frouin and B. Chatenet, 2000: A study of global aerosol optical climatology with two-channel AVHRR remote sensing. *J. Climate*, **13**, 2011–2027.

Hudson, J.G. and P.R. Frisbie, 1991: Cloud condensation nuclei near marine stratus. *J. Geophys. Res*., **96**, D11, 20795–20808.

——— and H. Li, 1995: Notes and correspondence. Microphysical contrasts in Atlantic stratus. *J. Atmos. Sci*., **52**, 3031–3040.

——— and S.S. Yum, 1997: Droplet spectral broadening in maritime stratus. *J. Atmos. Sci*., **54**, 2642–2654.

——— and ———, 2001: Maritime-continental drizzle contrasts in small cumuli. *J. Atmos. Sci.*, **15**, 915–926.

IPCC, 2001: Climate Change 2001: The scientific bases. [Houghton, J.T., Y. Ding, D.J. Griggs, M. Noguer, P.J. van der Linden, X. Dai, K. Maskel and C.A. Johnson (eds.)] Cambridge University Press, Cambridge, United Kingdom and New York, NY, USA, 881pp.

Kawamoto, K., 1999: On the global distribution of the water cloud microphysics derived from AVHRR remote sensing, Ph.D. thesis, University of Tokyo.

Kneizys, F.X., E.P. Shettle, L.W. Abreu, J.H. Chetwynd, G.P. Anderson, W.O. Gallery, J.E.A. Selby and S.A. Clough, 1988: Users Guide to LOWTRAN 7. Air Force Geophys. Lab. Tech. Rep. AFGL-TR-88-0177. 137pp.

Kovetz, A. and B. Olund, 1961: The effect of coalescence and condensation on rain formation in a cloud of finite vertical extent. *J. Atmos. Sci*., **26**, 1060–1065.

Laaksonen, A., P. Korhonen, M. Kulmala and R.J. Charlson, 1998: Modification of the Köhler equation to include soluble trace gases and slightly soluble substances. *J. Atmos. Sci*., **55**, 853–862.

Martin, G.M., D.W. Johnson and A. Spice, 1994: The measurement and parameterization of effective radius of droplets in warm stratocumulus clouds. *J. Atmos. Sci*., **51**, 1823–1842.

Mordy, W.A., 1959: Computations of the growth by condensation of a population of cloud droplets. *Tellus*, **11**, 16–44.

Nakajima, T. and M. Tanaka, 1986: Matrix formulations for the transfer of solar radiation in a plane-parallel scattering atmosphere. *J. Quant. Spectrosc. Radiat. Transfer*, **35**, 13–21.

——— and ———, 1988: Algorithms for radiative intensity calculations in moderately thick atmospheres using a truncation approximation. *J. Quant. Spectrosc. Radiat. Transfer*, **40**, 51–69.

———, A. Higurashi, K. Kawamoto and J.E. Penner, 2001: A possible correlation between satellite-derived cloud and aerosol microphysical parameters. *Geophys. Res. Lett*., **28**, 1171–1174.

Robinson, N.F., 1984: The efficient numerical calculation of condensational cloud drop growth. *J. Atmos. Sci*., **41**, 698–700.

Slingo, A., 1989: A GCM parameterization for the shortwave radiative properties of water clouds. *J. Atmos. Sci*., **46**, 1419–1427.

Stephens, G.L., 1978: Radiation profiles in extended water clouds. II: Parameterization schemes. *J. Atmos. Sci*., **35**, 2123–2132.

Takeda, T. and N. Kuba, 1982: Numerical study of the effect of CCN on the size distribution of cloud droplets. Part I. Cloud droplets in the stage of condensation growth. *J. Meteor. Soc. Japan*, **60**, 4, 978–993.

Taylor, J., M.D. Glew, J.A. Coakley Jr., W.R. Tahnk, S. Platnick, P.V. Hobbs and R.J. Ferek, 2000: Effect of aerosols on the radiative properties of clouds. *J. Atmos. Sci*., **57**, 2526–2670.

Twomey, S., 1959: The nuclei of natural cloud formation, Part II: The supersaturation in natural clouds and the variation of cloud droplet concentration. *Geofis. Pura. Appl*., **43**, 243–249.

———, 1974: Pollution and the planetary albedo. *Atmos. Environ*., **8**, 1251–1256.

———, 1977: The influence of pollution on the shortwave albedo of clouds. *J. Atmos. Sci*., **34**, 1149–1152.

———, 1991: Aerosol, clouds and radiation. *Atmos. Environ*., **25A**, 2435–2442.

Walcek, C.J. and N.M. Aleksic, 1998: A simple but accurate mass conservative, peak-preserving, mixing ratio bounded advection algorithm with FORTRAN code. *Atmos. Environ*., **32**, 3863–3880.

Yun, S.S. and J. Hudson, 2002: Maritime/continental microphysical contrasts in stratus. *Tellus*, **54B**, 61–73.